Advanced Composite Materials
Publication details, including instructions for authors and subscription information:
http://www.tandfonline.com/loi/tacm20

Crack modeling of steel-carbon hybrid FRCCs

Sung-Gul Hong [a] & Kyoung-Kyu Choi [b]

[a] Department of Architecture, Seoul National University, San 56-1, Shinlim-dong, Kwanak-gu, Seoul, 151-742, Korea

[b] School of Architecture, Soongsil University, 511, Sangdo-dong, Dongjak-gu, Seoul, 156-743, Korea

Version of record first published: 19 Oct 2012.

To cite this article: Sung-Gul Hong & Kyoung-Kyu Choi (2012): Crack modeling of steel-carbon hybrid FRCCs, Advanced Composite Materials, 21:4, 283-298

To link to this article: http://dx.doi.org/10.1080/09243046.2012.736345

Advanced Composite Materials
Vol. 21, No. 4, August 2012, 283–298

Taylor & Francis
Taylor & Francis Group

Crack modeling of steel–carbon hybrid FRCCs

Sung-Gul Hong[a] and Kyoung-Kyu Choi[b]*

[a]*Department of Architecture, Seoul National University, San 56-1, Shinlim-dong, Kwanak-gu, Seoul 151-742, Korea;* [b]*School of Architecture, Soongsil University, 511, Sangdo-dong, Dongjak-gu, Seoul 156-743, Korea*

(*Received 11 November 2010; accepted 14 February 2012*)

An experimental study to investigate nonlinear material behavior in tension of steel–carbon hybrid fiber reinforced cementitious composites (FRCC) was performed. In the tests, tensile strength, toughness index, and fracture properties, including fracture energy and crack opening or elongation, were measured. Based on the test results, a fictitious crack model for steel–carbon hybrid FRCC was developed. The proposed crack model was verified by comparing its predictions with the test results. Acceptable accuracy in simulating the tensile behavior of steel–carbon hybrid FRCC was obtained. For convenience in design and structure analysis, simplified equations to predict tensile strength and fracture energy in hybrid FRCC were developed.

Keywords: fiber reinforced cementitious composites (FRCC); steel fiber; carbon fiber; hybrid FRCC; crack model; tensile strength

1. Introduction

From ancient times, unprocessed natural fibers, such as straws, horse hairs, and bamboos, have been used as reinforcing materials of earthen construction materials including mud bricks and mortar (ACI 544.1R [1]). Such fibers can enhance the properties and reliability of construction materials. Recently, advances in construction and material technologies have enabled the use of high-performance engineered fibers, including synthetic and steel types, instead of crude natural fibers.

According to studies performed by ACI 544.1R [1], Naaman [2] and Li [3], the addition of fibers into concrete can significantly enhance material properties, including tensile and compressive strengths, flexural toughness, impact resistance, and fracture energy [4]. This is mainly a result of fibers transferring significant residual tensile stress across crack surfaces, even after tensile cracks develop in the matrix. In the steel fiber reinforce mortar in compression, the compressive strength and the strain corresponding to the compressive strength are increased, and the descending branch in the stress-strain curve shows more ductile behavior than that of the plain mortar [5]. Furthermore, the use of FRCC significantly improves flexural and shear strengths of cementitious structures [6–8]. It was also reported that fibers can reduce shrinkage cracking and crack widths in concrete [9–13] which can contribute to durability of the concrete [14]. Khuntia et al. [15] found, when using steel fibers in high-strength concrete, that the enhanced tensile strength of FRCC makes the failure mode more ductile.

*Corresponding author. Email: kkchoi@ssu.ac.kr

ISSN 0924-3046 print/ISSN 1568-5519 online

http://dx.doi.org/10.1080/09243046.2012.736345
http://www.tandfonline.com

Swamy et al. [16] performed experimental studies investigating the effect of steel fibers on the shear resistance of concrete beams containing steel fibers, 0–1% by volume. From the test, it was found that the addition of fibers can enhance the ultimate shear strength by 60–200%, and a truss model applicable to both lightweight and normal weight concrete beams was developed.

Naaman [2] reported that the primary fiber parameters that affect the material properties of FRCC are fiber aspect ratio (L_f/d_f), volume ratio (V_f), and fiber–matrix interfacial bond stress (τ), where L_f and d_f are fiber length and fiber diameter, respectively. Based on previous studies, ACI 544 [17] and RILEM TC 162 [18] have proposed design equations, which can evaluate nominal moment strength and shear strength of FRCC structures, defined using primary design parameters as functions. Theodorakopoulos and Swamy [19] and Harajli et al. [20] investigated the use of the steel fibers in the slab–column connections as shear reinforcement because the conventional shear reinforcement using stirrups is impractical due to the thin slab thickness. In their test, it was found that the punching shear strength can increase almost linearly with the steel fiber content, and the design equation to predict the punching shear strength of slab–column connections containing steel fiber was developed. Based on the advantages of FRCC, it has been used in various construction areas: airport paving [21], industrial flooring [22], and bridge deck overlays [23].

Recently, instead of conventional FRCC using a single type of fibers, there has been growing interest in hybrid FRCC (HFRCC) using two or more fiber types. Banthia and Sheng [24] and Kobayashi and Cho [25] performed experimental studies to investigate the behavioral characteristics of steel and carbon HFRCC and steel and polypropylene HFRCC, respectively. Their results showed that the use of HFRCC can enhance both material properties and structural capacities. Lawler, Zampini, and Shah [26] and Weiss and Shah [27] also performed extensive research to investigate the permeability and the cracking characteristics of hybrid fiber reinforced mortar. The test results contributed to quantify the crack damage (i.e. plastic shrinkage and restrained shrinkage cracking) and to use the hybrid fiber reinforcement for the purpose of cracking control of concrete structures. Yao et al. [28] found that the use of different fiber types with different fiber lengths can increase the tensile strength of concrete, and is effective for crack control for both micro-cracks and macro-cracks (Lawler et al. [26]). Recently, Johnston [29], Song and Hwang [30], and Arisoy and Wu [31] also found that the use of steel–polyvinyl alcohol (PVA) hybrid fibers can enhance the workability in concrete mixing and the material strength and deformability as well.

On the other hand, among the synthetic fibers, carbon fibers may not be used widely since they are relatively expensive. However, carbon fibers have various attractive material advantages (e.g. high tensile strength, elastic modulus, fire resistance, and long-term durability), and are inert to various chemicals (ACI 544.1R-96 [1]). Li and Obla [32] performed experimental and theoretical studies investigating the fiber length variation effect in carbon fiber cement composites. To utilize the advantages of carbon fibers in civil engineering application, further laboratory researches need to be continued to investigate the material properties of carbon fibers when used in hybrid FRCCs like steel–carbon hybrid fibers.

However, to date, limited experimental and theoretical studies on steel–carbon hybrid fibers have been reported. In addition, the applicability of current crack models, such as the German stress–strain model (DIN [33]) and the RILEM TC 162 [18] model, to HFRCC has not yet been confirmed by tests on HFRCC. Therefore, further studies were necessary to understand the material properties of HFRCC and to analyze structural behaviors when using HFRCC.

In the present study, a direct tension test was performed to investigate nonlinear material behavior of a HFRCC showing quasi-brittle behavior. Based on the experimental

observations, a fictitious crack model, simulating a tensile stress–crack-opening relationship, was developed. In the development of the crack model, the fracture mechanism of HFRCC and the effects of varying steel and carbon content in the HFRCC were addressed. The developed crack model was verified by comparing predictions with test results. For ease of application of the crack model in structure analysis and design, simplified equations for predicting and evaluating tensile strength and fracture energy were developed.

2. Test program

Experimental investigation of the tensile behavior of a steel–carbon HFRCC was performed using the direct tension test method described below.

2.1. Material

For mortar, a commonly used mix was employed. The mortar mix comprised: fine aggregate (river sand), 1246 kg/m^3; Type I Portland cement (Hanil Cement Co., Seoul, Korea), 745 kg/m^3; and water, 298 kg/m^3. According to the manufacturer's data sheets, the cement's specific gravity was 3.15 and its specific surface area was 320 m^2/kg. A high-range water reduction agent Mighty 150 (Kao Co., Japan) acted as a plasticizer. The mortar mix details are designed to achieve a 28 day compressive strength of mortar of 25–30 MPa and presented in Table 1.

Smooth, brass-coated hooked-end steel fibers (S) were used (Figure 1). The diameter (d_f), length (L_f), and aspect ratio (L_f/d_f) were 0.5 , 30 , and 60 mm, respectively. The steel fiber's tensile yield strength was 1176 N/mm^2. Carbon fibers (C) with d_f of 7 m, L_f of 6 mm, L_f/d_f of 857, and tensile strength of 4067 N/mm^2 were used (Figure 1).

Table 1. Mix proportion of mortar.

Mean compressive test strength (MPa)	*W/C* (%)	Unit content, kg/m^3				Slump (mm)	Air content (%)
		Water	Cement	Fine agg.	Admixture		
27.0	40.0	298	745	1246	2.2	190	3.0

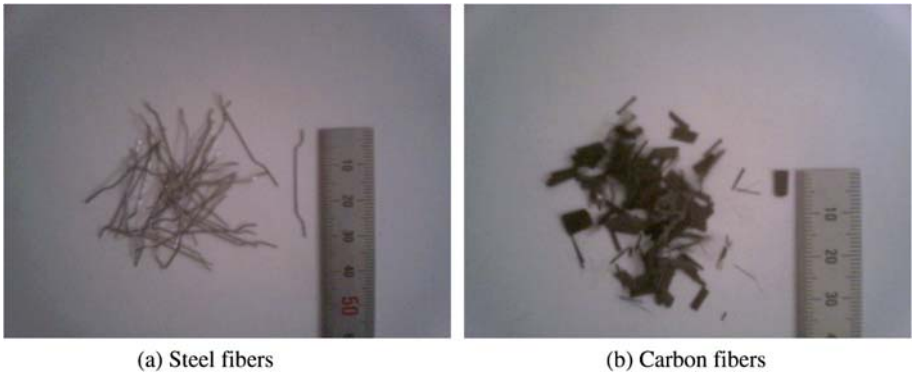

(a) Steel fibers (b) Carbon fibers

Figure 1. Steel and carbon fibers used in test.

A standard pan mixer was used to mix cement, water, plasticizer, and fibers. First, sand and cement were added by weight. Then, water was added and mixed for 5 min to form a uniform mix. Next, fibers were added, by weight, gradually to the mix. For improved mixing, plasticizer was added. Subsequently, mixing continued for 10 min to ensure that the fibers were uniformly dispersed in the mixture. Three (100×200) mm cylinders were cast from a batch without fibers, and tested to determine compressive strength. The mean compressive strength of the concrete cylinders after 28 days was 27.0 MPa. Three replicas of tensile test specimens were cast from each batch. In each batch, different proportion of steel and carbon fibers was used. All cast specimens were vibrated by using a table vibrator. Following casting, the specimens were covered with plastic sheets for one day prior to mold removal. Before load testing, the specimens were cured for 14 days in a water bath, then stored for another 14 days in ambient air at 20 ± 2 °C with a relative humidity of 65%.

2.2. *Direct tension tests*

Thirty-three specimens were prepared for direct tension testing using the apparatus shown in Figure 2. The tensile behavior of the test specimens, including initial stiffness, tensile strength, fracture energy, and crack opening, were assessed. A displacement-controlled test machine (actuator) with a loading capacity of 500 kN was used. To measure tensile behavior, loads were applied at low load rates of 0.5 mm/min (after Naaman and Baccouche [34]) and 1.0 mm/min, for displacements of 0–1 and 1–15 mm, respectively. Tests were performed at 20 ± 5 °C.

Details of dimensions and material properties of the test specimens are presented in Figure 3 and in Tables 1 and 2. The test specimens were ($150 \times 150 \times 500$) mm and at its center, the specimens had a 60 mm deep and 3 mm wide pre-crack notch. The load was applied 125 mm from the top and bottom edges of the specimens as shown in Figures 2 and 3. Details on the steel joint connecting the specimens and the actuator are presented in Figures 2 and 4.

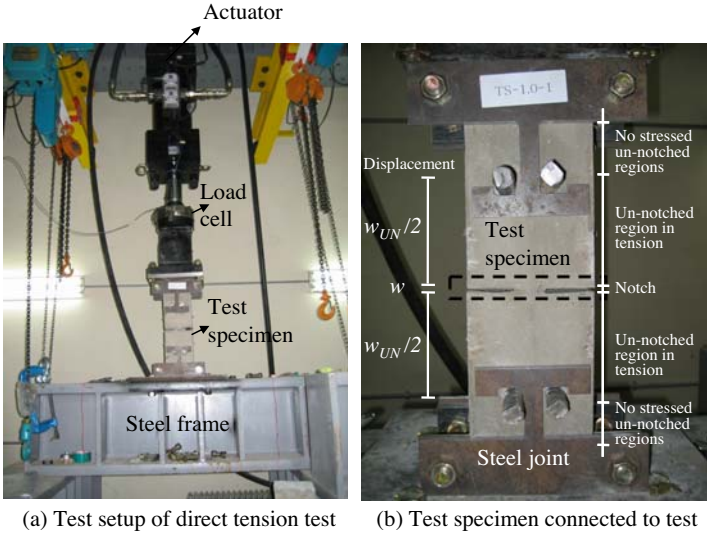

(a) Test setup of direct tension test

(b) Test specimen connected to test machine through steel joint

Figure 2. Direct tension test setup and specimen.

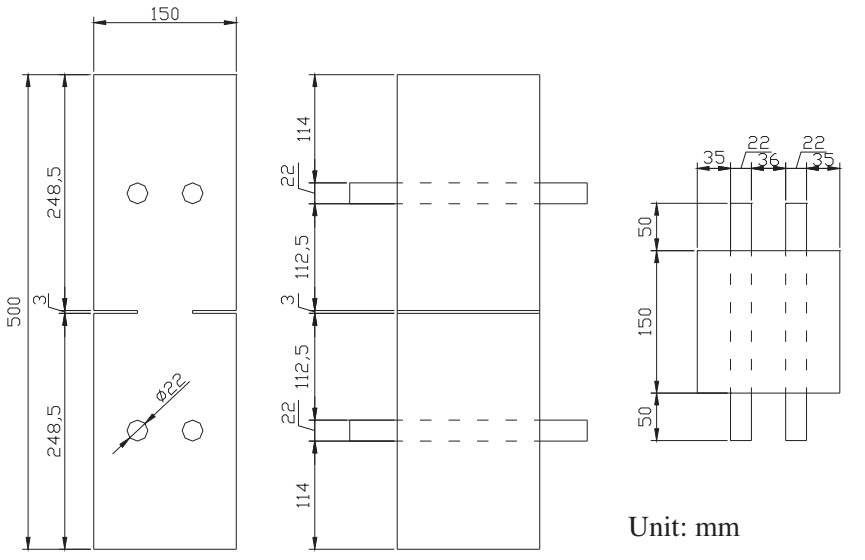

Figure 3. Details and dimensions of test specimen.

Table 2. Properties of test specimens.

Specimens	Total fiber volume ratio (%)	Steel vs. carbon fiber content
Training group		
M	0	NA
C-1.5	1.5	0: 1
S-1.5	1.5	1: 0
Validation group		
S1C5-1.5	1.5	1: 5
S1C4-1.5	1.5	1: 4
S1C3-1.5	1.5	1: 3
S1C2-1.5	1.5	1: 2
S1C1-1.5	1.5	1: 1
S2C1-1.5	1.5	2: 1
S3C1-1.5	1.5	3: 1
S4C1-1.5	1.5	4: 1
S5C1-1.5	1.5	5: 1
S1C1-1	1.0	1: 1

NA: not applicable.

In the direct tension test, two primary parameters were varied: the total volume ratio of fibers and the proportions of steel and carbon fibers within a given total volume ratio of fibers. Three total volume ratios were used: 0, 1.0, and 1.5%. The test specimen with 0% fiber was plain mortar. Two FRCC specimens, each containing only steel or carbon fibers, were tested. Thirty specimens containing both steel and carbon fibers, and with different proportions of each fiber, were tested to assess the effects of different steel and carbon fiber volume ratios on tensile behavior of steel–carbon HFRCC.

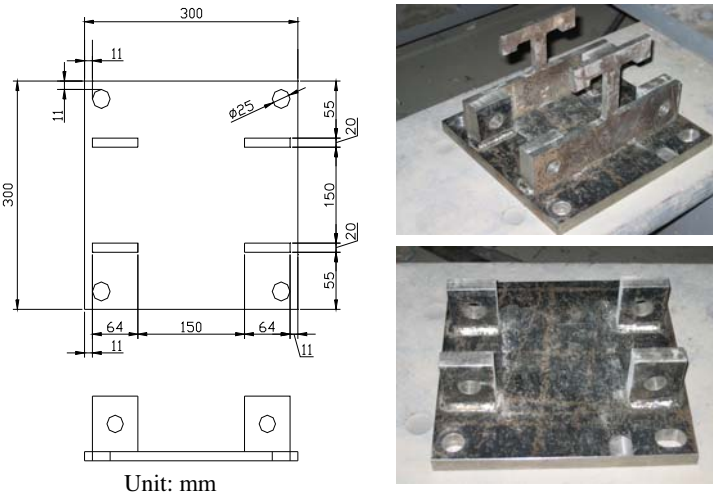

Figure 4. Steel joint details connecting test machine and specimen.

3. Test results and discussion

FRCC showing a quasi-brittle behavior usually fails in a pure opening mode called Mode I [35], and has a wide energy absorption zone with numerous micro-cracking [16]. Their failure modes are typically rather ductile compared to conventional concrete [22]. Thus, fracture energy per unit area (G_f) and crack opening data are necessary to explain the nonlinear fracture mechanism of FRCC.

In this study, instead of using a conventional three-point bending test, a direct tension test was performed to investigate the tensile behavior including the fracture energy of steel–carbon HFRCC. The test specimens had a central notch to simulate a pre-crack locale and damage localization of the FRC materials. In the present study, the deformation at the notched cross section (w) was evaluated by subtracting the elastic deformation (w_{UN}) in the unnotched region from the total deformation (w_T) of the whole specimen, which was acquired from the actuator (Figure 2): $w = w_T - w_{UN}$. In the unnotched region, deformation (w_{UN}) was insignificant because that region's tensile stress level was relatively low compared to that in the notched region, and it was evaluated based on the elasticity theory (Figure 2(b)). It should also be noted that the acquired test data from the actuator were corrected to compensate the initial slip of the test specimens and set-up at the early loading stage.

Figure 5 illustrates the formation of cracking patterns around the notched region of test specimens: C-1.5, S-1.5, and S5C1-1.5. In C-1.5 having carbon fibers, one major tensile crack developed within the notched region, and the carbon fibers were evenly distributed throughout the cross section of notched region. In S-1.5 having steel fibers, entire notched region cracked severely and unnotched region also suffered significant cracking damage. The S5C1-1.5 having both steel and carbon fibers shows almost a similar cracking pattern to S-1.5.

Figure 6 shows the tensile stress–displacement behavior of two test specimens: S5C1-1.5 having more steel fibers than carbon fibers (S to C fiber ratio was 5:1) and S1C5-1.5 having less steel fibers than carbon fibers (S to C fiber ratio was 1:5). The other material properties, including total fiber volume ratio (1.5%), were similar. The tensile strength, σ_t, was evaluated in the unnotched area (30×150 mm) shown in Figure 3. As shown in Figure 6, the S5C1-1.5 has a higher tensile strength than S1C5-1.5. In terms of tensile strength of FRCC, bond stress

(a) C-1.5

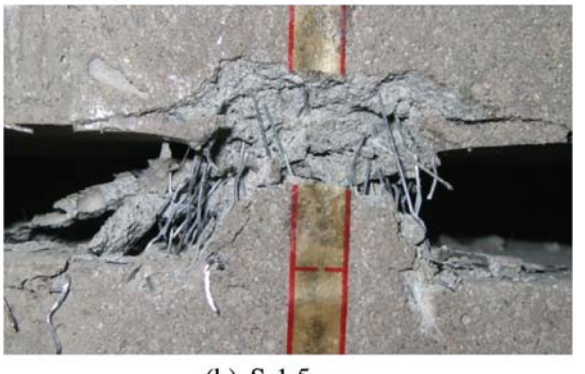

(b) S-1.5

(c) S5C1-1.5

Figure 5. Typical cracking patterns of test specimens: (a) C-15 (b) S-15 and (c) S5C1-1.5.

(τ) at fiber pullout failure is a key parameter [2,8]. As the bond stress value of steel fibers is significantly greater than that of carbon fibers (4.15 and 0.6 MPa, respectively; Bentur et al. [36]), the tensile strength of steel–carbon HFRCC is heavily dependent on the steel fiber content.

With regard to ductile tensile behavior, S1C5-1.5 with more carbon fibers exhibited greater ductile behavior than that shown by S5C1-1.5 with more steel fibers. This may be

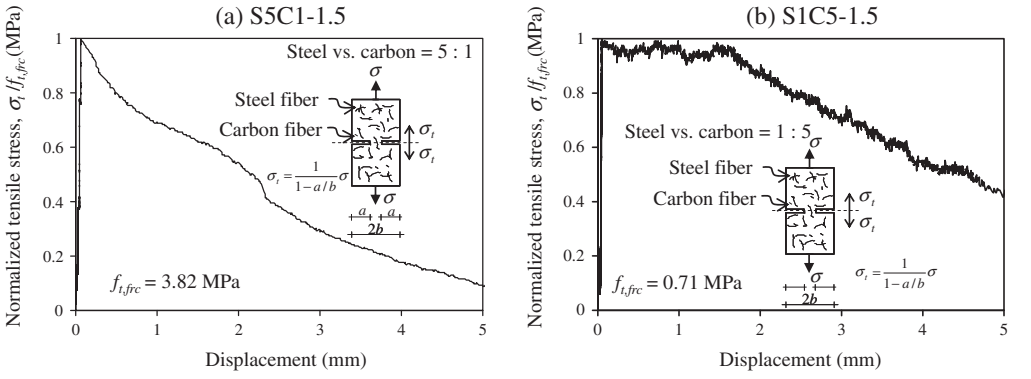

Figure 6. Tensile stress–displacement relationship of specimens S5C1-1.5 and S1C5-1.5.

explained by fiber size differences. Since the carbon fibers were micro-fibers with a short fiber length (6 mm) and small diameter (7 m), more carbon fibers than steel fibers could be located at crack surfaces. Across thin cracks, such micro-fibers can transfer significant tensile stress after peak tensile strength has been reached, which in turn produces the greater ductile tensile behavior of FRCC [36]. However, since the length of carbon fibers is short, they are not effective across macro-cracks. It has been reported that each fiber can transfer tensile stress until the maximum crack opening, approximately $L_f/2$, has developed [37]. Figure 7 shows the load–displacement relationship of test specimens, C-1.5 and S-1.5 (1.5% carbon or 1.5% steel fibers, respectively). As shown in Figure 7, at a small displacement, the C-1.5 FRCC specimen showed greater ductile tensile behavior compared to the S-1.5 FRCC specimen. However, the C-1.5 FRCC did not develop residual tensile stress at a large crack opening. The maximum displacement of C-1.5 and S-1.5 was approximately 1.3 and 12 mm, respectively, which in turn correspond to $L_f/4.6$ and $L_f/2.5$. Among the steel–carbon HFRCC specimens, the maximum displacement was approximately 12 mm, similar to that of our pure steel FRCC specimen (S-1.5).

In ASTM C1018 [38], the toughness index (I_n) is used to quantify the toughness of FRCC at a given deformation. Here, I_n is defined as the ratio of the area under the load–deflection curve at $(n+1)/2$ times the first-cracking deflection to the area under the load–

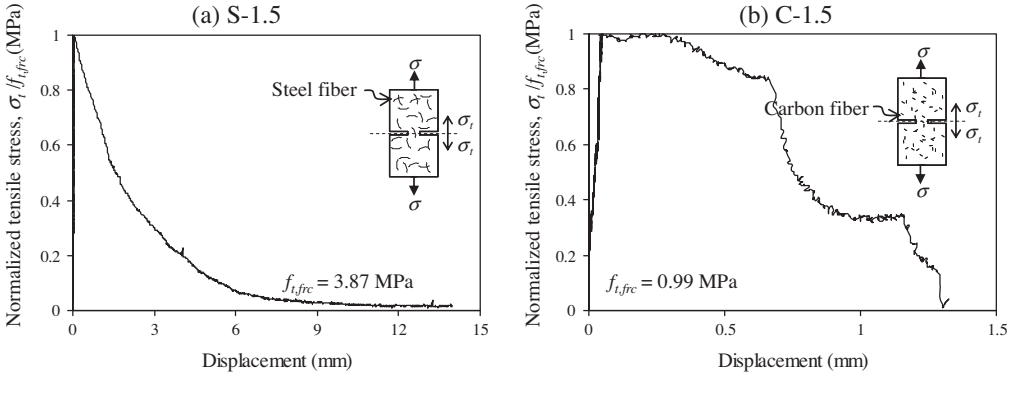

Figure 7. Tensile stress–displacement relationship of specimens S-1.5 and C-1.5.

deflection curve at the first-cracking deflection. To investigate the tensile behavior of the HFRCC test specimens, toughness indices were calculated. As shown in Table 3, the I_{100} of S1C5-1.5 and S5C1-1.5 were 130.3 and 43.0, respectively. As expected, the toughness index of S1C5-1.5 with more carbon fibers was greater than that of S5C1-1.5 with more steel fibers. Toughness indices for all specimens are presented in Table 3 and Figure 8(a). The results show that as carbon fiber content increases, the toughness index (I_{100}) increases.

Figures 8(b) and (c) present the tensile strength and fracture energy (G_f) of those test specimens with a total fiber volume ratio of 1.5%. The figure shows that with increasing steel fiber content, tensile strength and fracture energy increase. Since steel fibers have a high bond stress, they can enhance the tensile strength of HFRCC. At a large crack opening, the steel fibers with the longer fiber length (30 mm) can work effectively while the carbon micro-fibers with short fiber lengths (6 mm) were not effective. *It should be noted that the toughness indices and fracture energy acquired from test results showed wide deviations, which was partly due to the large loading capacity of the machine (500 kN) while the maximum applied load was under 25 kN.*

Table 3. Toughness index, tensile strength, fracture energy, and characteristic length obtained from tension test and predicted by proposed model.

	Test results			Proposed method	
Specimens	Toughness index, I_{100}	Tensile strength, $f_{t,frc}$ (MPa)	Fracture energy, $G_{f,frc}$ (MPa m)	Tensile strength, $f_{t,frc}$ (MPa)	Fracture energy, $G_{f,frc}$ (MPa m)
S1C5-1.5	130.3	2.02	5.71E−03	1.45	5.30E−03
	112.4	0.71	3.52E−03		
S1C4-1.5	76.6	1.82	7.50E−03	1.53	5.54E−03
S1C3-1.5	72.8	2.19	5.67E−03	1.67	5.89E−03
	143.6	1.20	5.87E−03		
	75.1	2.54	6.84E−03		
S1C2-1.5	81.2	2.33	1.05E−02	1.88	6.42E−03
	58.5	1.75	6.58E−03		
S1C1-1.5	76.0	1.42	7.63E−03	2.32	7.32E−03
	104.9	3.33	8.29E−03		
	55.9	1.49	4.23E−03		
S2C1-1.5	25.9	3.31	8.20E−03	2.75	8.00E−03
	68.8	1.64	4.57E−03		
S3C1-1.5	52.0	3.32	1.10E−02	2.97	8.26E−03
	74.9	2.16	9.24E−03		
	38.6	1.77	4.70E−03		
S4C1-1.5	61.2	3.21	7.04E−03	3.10	8.38E−03
	99.1	4.08	1.66E−02		
	57.3	4.45	1.00E−02		
S5C1-1.5	43.0	4.62	1.64E−02	3.19	8.46E−03
	82.9	3.82	8.83E−03		
S1C1-1	82.7	1.05	6.50E−03	1.88	5.22E−03
	48.0	1.74	5.62E−03		
	71.5	1.88	6.33E−03		
Mean[a]				1.04	1.13
SD[a]				0.189	0.238

[a]Mean and standard deviation of the ratio of the tensile strength (or fracture energy) obtained from experimental results and predicted by proposed method.

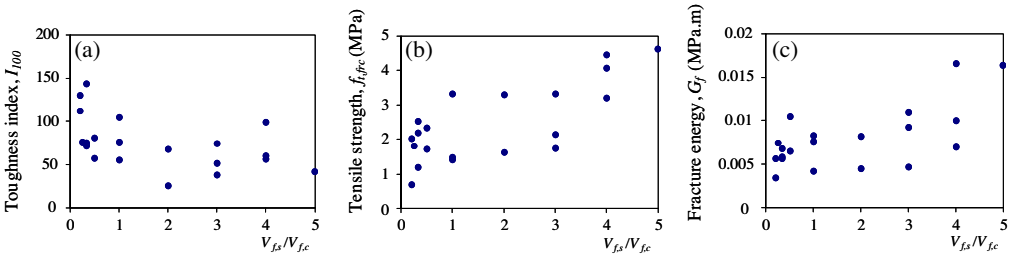

Figure 8. Variation of toughness index, tensile strength, and fracture energy according to the fiber volume ratio between steel and carbon fibers.

Based on these limited experimental observations, it is concluded that steel fiber content is a primary parameter in determining fracture energy (G_f) and tensile strength, while carbon fiber content is a primary parameter determining toughness index.

4. Model development and validation

4.1. *Fictitious crack model for steel-carbon HFRCC*

A fictitious crack model has been used to simulate the progressive fracture process including strain and damage localization [39,40]. This method can be used to describe the near-tip nonlinear zone as well as the concrete fracture process when pre-cracks are present (Bazant and Planas [35]). In this crack model, the cohesive stress ($\sigma(w)$) after a peak load, which is transferrable across a cohesive crack, was a function of the crack opening (w) as shown in Figure 9 and Equation (1).

$$\sigma = f(w) \tag{1}$$

The fictitious crack model can be used as a constitutive relation in structural analysis [35] and can connect classic mechanics based on strength with fracture mechanics based on energy. In this study, neglecting the bulk dissipation energy (G_I) developed during unloading of tensile stress after tensile cracking occurs, a simplified bi-linear fictitious crack model [18,39,40], with three material parameters (w_m,w_c, and α), was modified for application to steel or carbon FRCC.

$$\sigma = f_{t,frc} + [(\alpha - 1)f_{t,frc}/w_c]w \quad \text{for } w \le w_c \tag{2a}$$

$$\sigma = [\alpha f_{t,frc}/(w_m - w_c)] \cdot (w_m - w) \quad \text{for } w_c < w \le w_m \tag{2b}$$

where, $f_{t,frc}$ is the tensile strength of the FRCC, w_m is the maximum crack opening, and α and w_c are modeling parameters. The bi-linear crack model is expected to be conveniently used in design practice.

Our data were divided into two groups: a training group for determining the modeling parameters of the crack model and a testing group for validating the proposed model. The training group included three test specimens: specimen M without fibers; specimen S-1.5 containing 1.5% steel fibers; and specimen C-1.5 containing 1.5% carbon fibers. The remaining 30 test specimens were used in the testing group for verification of the model.

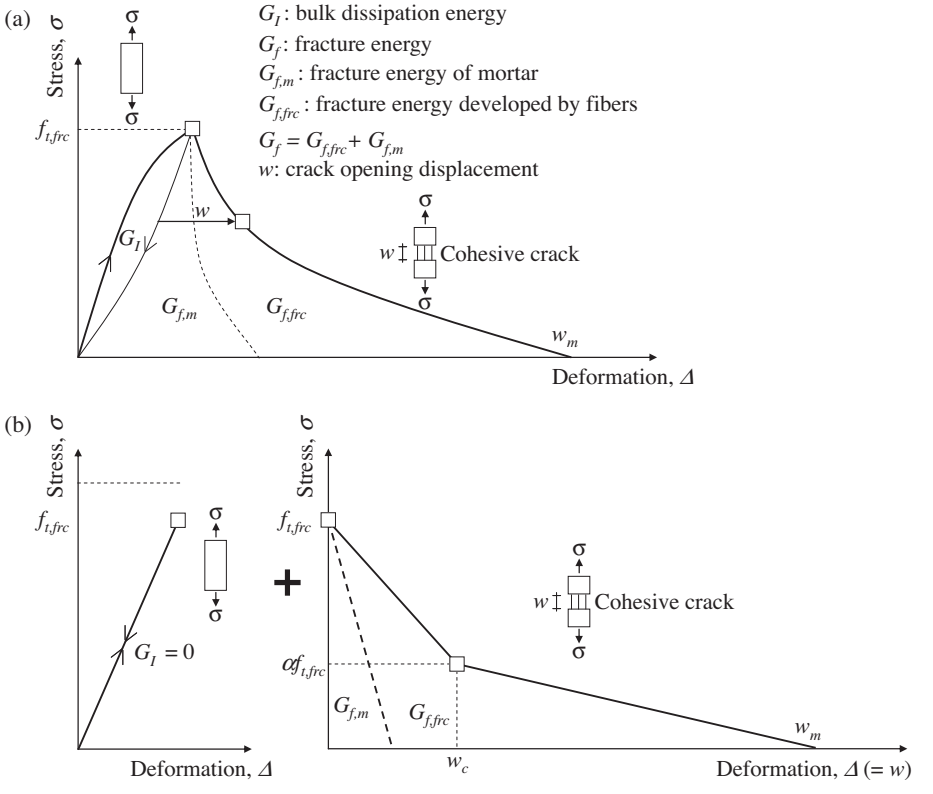

Figure 9. Tensile stress–deformation relationship of HFRC: (a) realistic tensile stress–deformation, (b) idealized tensile stress–deformation (crack opening) in fictitious crack model [35].

For specimen M, the tensile strength (f_t) and the fracture energy $G_{f,m}$) were 1.02 and 3.30×10^{-5} MPa m, respectively. In the S-1.5 specimen, the tensile strength ($f_{t,frc}$) and the fracture energy (G_f) were 3.87 and 9.28×10^{-3} MPa m, respectively, while the tensile strength ($f_{t,frc}$) and the fracture energy ((G_f) in C-1.5 were 0.82 and 5.20×10^{-4} MPa m, respectively. The results indicate that the fracture energy of M is insignificant compared to those of steel or carbon FRCC. Based on these observations, the modeling parameter, α, was evaluated so that the proposed crack model using the above modeling parameters produced fracture energies identical to those obtained from the test results on M, S-1.5, and C-1.5. The parameter was determined by

$$\alpha = (G_f - f_{t,frc} w_c/2)/(f_{t,frc} w_m/2) \tag{3}$$

where, $G_f = [G_{f,m} + G_{f,frc}]$ is the sum of the fracture energy of M ($G_{f,m}$) and that developed by either steel or carbon fibers ($G_{f,frc}$). From Equation (3), α values of S-1.5 FRCC and C-1.5 FRCC were 0.08 and 0.38, respectively. It should be noted that the fracture energy of M ($G_{f,m}$) was obtained from test results while the fracture energy developed by either steel or carbon fibers ($G_{f,frc}$) was evaluated by subtracting $G_{f,m}$ from the total fracture energy (G_f) of S or C series of test specimens. In addition, for simplicity, the bulk dissipation energy G_I was assumed to be zero.

The proposed fictitious crack model shown in Equation (2) was also used for the steel–carbon HFRCC specimens. However, prior to the predictions, tensile strengths and the three modeling parameters (w_m,w_c, and α) for steel–carbon HFRCC were required. For simplicity, w_m and w_c of the steel–carbon HFRCC were defined to be constants, $w_m = L_f/3 = 10\,\text{mm}$ and $w_c = 0.40 \cdot w_m = 4\,\text{mm}$ based on least square techniques to obtain minimum root mean square prediction error after Fan and Yuan [41]. The w_m of the steel–carbon HFRCC was defined to be 10 mm for all tested HFRCC specimens regardless of the proportion of steel and carbon fibers in the specimens (see Figure 10). Neglecting the possible interactions between steel and carbon, the α value of steel–carbon HFRCC specimens were based on the superposition principle and determined by

$$\alpha = \frac{\sum V_{f,i}\alpha_i}{V_{fo}} \tag{4}$$

where, i is s or c indicating steel or carbon FRCC, $V_{f,i}$ is the fiber volume ratio of the steel or carbon FRCC, V_{fo} (=0.015) is the fiber volume ratio of the test specimen used during crack model training, and from the above, $\alpha_s = 0.08$ and $\alpha_c = 0.38$.

Based on the Naaman and Reinhardt [42] model, the tensile strength of HFRCC may be defined as

$$f_{t,frc} = f_t(1 - V_f) + V_{f,s}\tau_s\frac{L_s}{d_s}\alpha_1\alpha_2 \tag{5}$$

where, τ_s is a steel fiber–matrix interfacial bond stress (4.15 MPa) [42], α_1 is a coefficient representing the fraction of a bond mobilized at first matrix cracking, and α_2 is the efficiency factor of fiber orientation in the uncracked state of the composite. For simplicity, $\alpha_1 = 1.0$ and $\alpha_2 = 0.7$ [36] were used. Tensile strength of the matrix, f_t is $0.166\sqrt{f'_c}$ (MPa) based on the test results for specimen M. It should be noted that in Equation (5), the contribution of carbon fiber to the tensile strength of HFRCC was neglected because the tensile strengths of the specimens M and C-1.5 did not show a significant difference.

4.2. Model validation

To verify the proposed fictitious crack model for steel–carbon HFRCC (Equations (2), (4), and (5)), its predictions were compared with test results. It should be noted that the specimens used during verification were not used in the development of the crack model. Figure 10 presents both experimental results and tensile stress–displacement relations predicted by the proposed crack model for 30 test specimens (validation group). Six test specimens were omitted from the validation as they failed prematurely due to unexpected damage.

As shown in Figure 10, the proposed crack model accurately simulated the stress–displacement relationship before and after cracking. In the proposed model (refer to Figure 9), fracture energy is evaluated as

$$G_f = (\alpha w_m + w_c)f_{t,frc}/2. \tag{6}$$

In Table 3, the predicted fracture energies calculated by Equation (6) are presented and compared with the test results. The mean and standard deviation of the ratios between the fracture energies obtained from experiments and those predicted by the proposed model (Equation (6)) were 1.13 and 0.238, respectively. In addition, the predicted tensile strengths

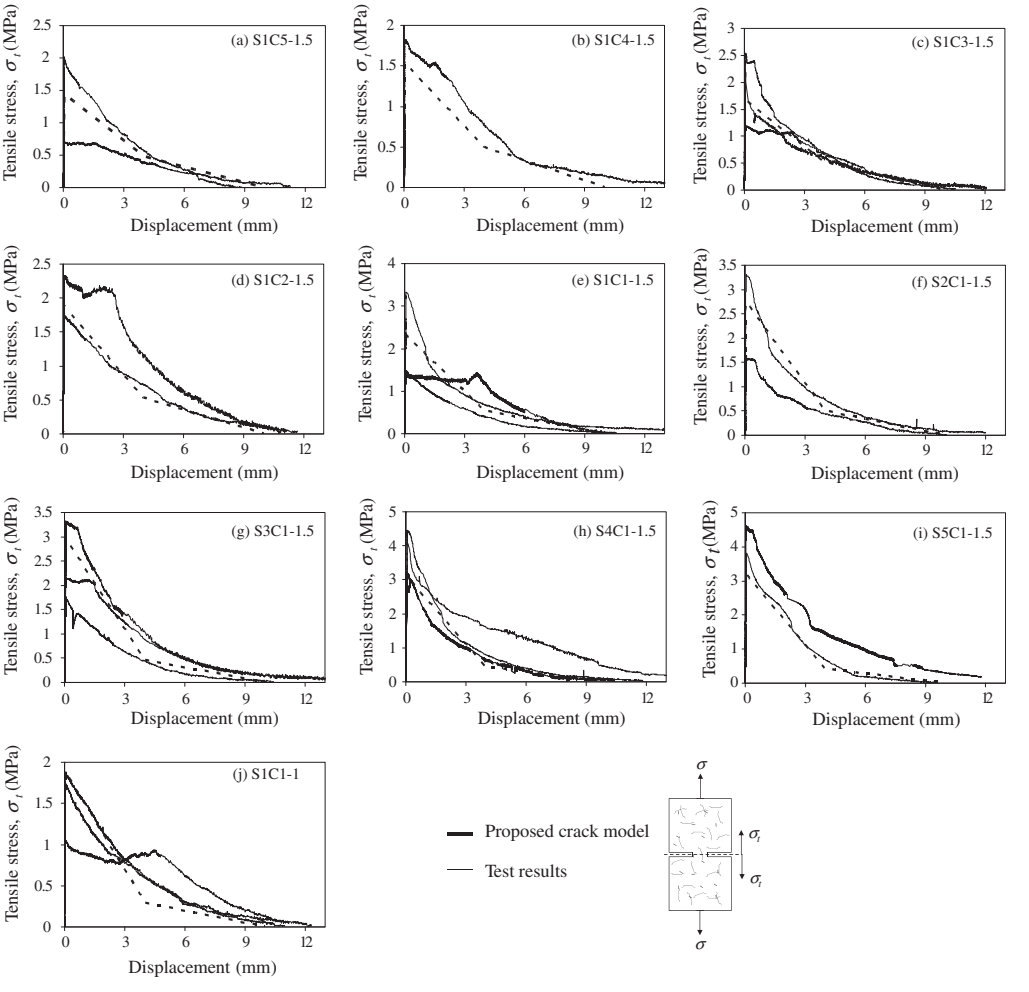

Figure 10. Prediction of tensile stress–displacement relationship of test specimens by using proposed crack model.

using Equation (4) are shown in Table 3. The mean and standard deviation of the ratios between the tensile strengths obtained from experiments and those predicted by the model are 1.04 and 0.189, respectively. The results show that the proposed fictitious crack model can predict tensile strength and fracture energy of steel–carbon HFRCC with acceptable accuracy. However, further investigation into the effects of fiber parameters (e.g. fiber aspect ratio and bond stress at pullout failure) and the combined effect of steel and carbon fibers on the tensile behavior of steel–carbon HFRCC are needed. Such investigations may improve the accuracy and precision of the proposed fictitious crack model and its modeling parameters.

5. Conclusions

Direct tension tests were performed to investigate the tensile behavior of steel and carbon FRCC and steel–carbon HFRCC. The results showed that carbon in FRCC contributes toughness in tensile behavior before reaching the maximum crack opening while steel in FRCC contributes

tensile strength. Further, as steel fiber content increased and carbon fiber content decreased, tensile strength showed an increase while the toughness index decreased. Since tensile behavior at large crack widths would be predominantly governed by the steel fibers, fracture energy would be mainly dependent on the steel fiber content rather than on the carbon fiber content.

Based on the experimental observations, a fictitious crack model was developed. The modeling parameters of the crack model were defined as functions of the fracture parameters obtained from the steel and carbon FRCC results. Our results verified that the proposed model can properly simulate the tensile behavior of steel–carbon HFRCC, and can predict tensile strength and fracture energy with acceptable accuracy. We suggest that the proposed crack model is suitable for use in finite element analysis for simulating realistic tensile behavior of steel–carbon HFRCC that exhibit quasi-brittle behavior. It is noted that this finding is based on direct tension test results only, and further investigation on fiber orientation effect is necessary to completely understand the tensile behavior of steel–carbon HFRCC.

Notations

d_f	fiber diameter
f_t	tensile strength of specimen M
$f_{t,frc}$	tensile strength of specimen C or S
G_f	fracture energy per unit area
$G_{f,m}$	fracture energy of specimen M
$G_{f,frc}$	fracture energy developed by either steel or carbon fibers
G_I	bulk dissipation energy developed during unloading of tensile stress after tensile cracking occurs
I_n	toughness index
L_f	fiber length
$L_{f/df}$	fiber aspect ratio
V_f	volume ratio
$V_{f,i}$	fiber volume ratio of the steel or carbon FRCC
V_{fo}	fiber volume ratio of the test specimen used during crack model training
w	crack opening
w_c	modeling parameter
w_m	maximum crack opening
α	modeling parameter
α_1	coefficient representing the fraction of a bond mobilized at first matrix cracking
α_2	efficiency factor of fiber orientation in the uncracked state of the composite
τ	fiber–matrix interfacial bond stress
τ_s	steel fiber–matrix interfacial bond stress
$\sigma(w)$	cohesive stress after a peak load

Acknowledgment

This paper has been financially supported by Basic Science Research Program through the National Research Foundation of Korea (NRF) funded by the Ministry of Education, Science and Technology (2012R1A1A2A04667943). This support is greatly acknowledged.

References

[1] ACI 544.1R. State-of-the-art report of fiber reinforced concrete. Farmington Hills: ACI Committee 544; 1996 [Reapproved in 2002].

[2] Naaman AE. Toughness, ductility, surface energy and deflection-hardening FRC composites. In: Proceedings of the JCI International workshop on Ductile Fiber Reinforced Cementitious Composites (DRFCC) – Application and Evaluation (DFRCC-2002); Japan Concrete Institute; 2002 Oct. p. 33–57.

[3] Li VC. From micromechanics to structural engineering-the design of cementitious composites for civil engineering applications. Struct. Eng./Earthquake Eng. 1993 Jul;10:37–48.
[4] Naaman AE, Likhitruangsilp V, Parra-Montesinos G. Punching shear response of high-performance fiber-reinforced cementitious composite slabs. ACI Struct. J. 2007;104:170–179.
[5] Shah SP, Stroeven P, Dalhuisen D, Van Stekelenburg P. Complete stress-strain curves for steel fibre reinforced concrete in uniaxial tension and compression. Testing and test methods of fibre cement composites. RILEM Symposium. Lancastre: Construction Press; 1978;399–408.
[6] Johnston CD. Definitions and measurement of flexural toughness parameters for fiber reinforced concrete. ASTM Cement Concrete Aggregates. 1982 Winter;4:53–60.
[7] Li VC, Ward R, Hamza AM. Steel and synthetic fibers as shear reinforcement. ACI Mater. J. 1992;89:499–508.
[8] Narayanan R, Darwish IYS. Use of steel fibers as shear reinforcement. ACI Struct. J. 1987;84:216–227.
[9] Malmberg B, Skarendahl A. Method of studying the cracking of fibre concrete under restrained shrinkage, testing and test methods of fibre cement composites. RILEM Symposium; Lancaster: Construction Press; 1978. p. 173–179.
[10] Naaman AE, Wongtanakitcharoen T, Hauser G. Influence of different fibers on plastic shrinkage cracking of concrete. ACI Mater. J. 2005;102:49–58.
[11] See HT, Attiogbe E, Miltenberger MA. Shrinkage cracking characteristics of concrete using ring specimens. ACI Mater. J. 2003;100:239–245.
[12] Moon J-H, Weiss J. Estimating residual stress in the restrained ring test under circumferential drying. Cement Concr. Compos. 2006;28:486–496.
[13] Moon J-H, Rajabipour F, Pease B, Weiss J. Quantifying the influence of specimen geometry on the results of the restrained ring test. J. ASTM Int. 2006;3:1–14.
[14] Schupack M. Durability of SRFC exposed to severe environments. In: Steel fiber concrete. Amsterdam: Elsevier; 1986. p. 479–496.
[15] Khuntia M, Stojadinovic B, Goel SC. Shear strength of normal and high-strength fiber reinforced concrete beams without stirrups. ACI Struct. J. 1999;96:282–289.
[16] Swamy RN, Jones R, Chiam ATP. Influence of steel fibers on the shear resistance of lightweight concrete I-beams. ACI Struct. J. 1993;90:103–114.
[17] ACI 544.4R. Design considerations for steel fiber reinforced concrete. Farmington Hills: ACI Committee 544; 1988 [Reapproved in 1999].
[18] RILEM TC 162-TDF. Design of steel fiber reinforced concrete using $\sigma - w$ method: principles and applications, RILEM TC 162-TDF: test and design methods for steel fiber reinforced concrete. Mater. Struct. 2002 June;35:262–278.
[19] Theodorakopoulos DD, Swamy RN. Contribution of steel fibers to the strength characteristics of lightweight concrete slab-column connections failing in punching shear. ACI Struct. J. 1993;90:342–354.
[20] Harajli MH, Maalouf D, Khatib H. Effect of fibers on the punching shear strength of slab-column connections. Cement Concr. Compos. 1995;17:161–170.
[21] Lankard DR, Schrader EK. Inspection and analysis of curl in steel fiber reinforced concrete airfield pavements. Bekaert Corp., Marietta; 1983 Apr:9.
[22] Robinson C, Colasanti A, Boyd G. Steel fiber reinforced auto assembly plant floor. Concr. Int. 1991 Apr;13:30–35.
[23] Scharader EK. Fiber reinforced concrete pavements and slabs – a state-of-the-art report. In: Steel fiber concrete. Amsterdam: Elsevier; 1986. p. 109–131.
[24] Banthia N, Sheng J. Micro-reinforced cementitious materials. Materials Research Society Symposium Proceedings; 1990 Nov; Boston. 211.
[25] Kobayashi K, Cho R. Flexural characteristics of steel fiber and polypropylene fiber hybrid reinforced concrete. Composites. 1982;13:164–168.
[26] Lawler J, Zampini D, Shah SP. Permeability of cracked hybrid fiber reinforced mortar under load. ACI Mater. J. 2002;99:379–385.
[27] Weiss WJ, Shah SP. Restrained shrinkage cracking: the role of shrinkage reducing admixtures and specimen geometry. Mater. Struct. 2002;17:85–91.
[28] Yao U, Li J, Wu K. Mechanical properties of hybrid fiber-reinforced concrete at low fiber fraction. Cement Concr. Res. 2003;33:27–30.
[29] Johnston CD. Steel fibre reinforced mortar and concrete – a review of mechanical properties. Fiber Reinforced Concr. SP-44, ACI. 1974:127–142.

[30] Song PS, Hwang S. Mechanical properties of high-strength steel fiber-reinforced concrete. Constr. Build. Mater. 2004;18:669–673.
[31] Arisoy B, Wu HC. Material characteristics of high performance lightweight concrete reinforced with PVA. Constr. Build. Mater. 2008;22:635–645.
[32] Li VC, Obla KH. Effect of fiber length variation on tensile properties of carbon-fiber cement composites. Compos. Eng. 1994;4:947–963.
[33] DIN 1045–1. Tragwerke aus Beton, Stahlbeton und Spannbeton - Teil 1: Bemessung und Konstruktion [Concrete, reinforced and prestressed concrete structures - Part 1: design and construction]. Betonkalender. Berlin: Ernst & Sohn; 1999.
[34] Naaman AE, Baccouche MR. Shear response of dowel reinforced SIFCON. ACI Struct. J. 1995;92:587–596.
[35] Bazant ZP, Planas J. Fracture and size effect in concrete and other quasibrittle materials. New York: CRC Press; 1998.
[36] Bentur A, Wu ST, Banthia N, Baggott R, Hansen W, Katz A, Leung CKY, Li VC, Mobasher B, Naaman AE, Robertson R, Soroushian P, Stang H, Taerwe LR. Fiber–matrix interfaces. In: Naaman AE, Reinhardt HW, editors. High performance fiber reinforced cement composites 2. London: E&FN Spon; 1996. p. 149–191.
[37] Li VC, Mihashi H, Wu HC, Alwan J, Brincker R, Horii H, Leung C, Maalej M, Stang H. Micromechanical models of mechanical response of HPFRCC. In: Naaman AE, Reinhardt HW, editors. High performance fiber reinforced cement composites 2. London: E&FN Spon; 1996. p. 43–52.
[38] ASTM C1018. Test method for flexural toughness and first crack strength of fiber reinforced concrete (using beam with third-point loading). West Conshohocken (PA): ASTM; 2005.
[39] Hillerborg A. Analysis of one single crack. In: Wittmann FH, editor. Fracture mechanics of concrete. Amsterdam: Elsevier, 1983. p. 223–249.
[40] Hillerborg A, Modeer M, Petersson PE. Analysis of crack formation and crack growth in concrete by means of fracture mechanics and finite elements. Cement Concr. Res. 1976;6:773–782.
[41] Fan JY, Yuan YX. On the convergence of a new Levenberg-Marquardt method. Technical Report. AMSS, Chinese Academy of Sciences; 2001. p. 11.
[42] Naaman AE, Reinhardt HW. Characterization of high performance fiber reinforced cement composites-HPFRCC. In: Naaman AE, Reinhardt HW, editors. High performance fiber reinforced cement composites 2. London: E&FN Spon; 1996. p. 1–24.